

Neuro-immune signatures in chronic low back pain subtypes

Zeynab Alshelh,¹ Ludovica Brusaferrri,¹ Atreyi Saha,¹ Erin Morrissey,¹ Paulina Knight,¹ Minhae Kim,¹ Yi Zhang,² Jacob M. Hooker,¹ Daniel Albrecht,¹ Angel Torrado-Carvajal,^{1,3} Michael S. Placzek,¹ Oluwaseun Akeju,² Julie Price,¹ Robert R. Edwards,⁴ Jeungchan Lee,¹ Roberta Sclocco,^{1,5} Ciprian Catana,¹ Vitaly Napadow^{1,4} and Marco L. Loggia¹

Abstract

We recently showed that patients with different chronic pain conditions (such as chronic low back pain, fibromyalgia, migraine, and Gulf War Illness) demonstrated elevated brain and/or spinal cord levels of the glial marker 18kDa translocator protein, which suggests that neuroinflammation might be a pervasive phenomenon observable across multiple etiologically heterogeneous pain disorders. Interestingly, the spatial distribution of this neuroinflammatory signal appears to exhibit a degree of disease specificity (e.g., with respect to the involvement of the primary somatosensory cortex), suggesting that different pain conditions may exhibit distinct “neuroinflammatory signatures”. To further explore this hypothesis, we tested whether neuroinflammatory signal can characterize putative etiological subtypes of chronic low back pain patients based on clinical presentation. Specifically, we explored neuroinflammation in patients whose chronic low back pain either did or did not radiate to the leg (i.e., “radicular” vs. “axial” back pain).

Fifty-four chronic low back pain patients, twenty-six with axial back pain (43.7 ± 16.6 y.o. [mean \pm SD]) and twenty-eight with radicular back pain (48.3 ± 13.2 y.o.), underwent PET/MRI with [¹¹C]PBR28, a second-generation radioligand for the 18kDa translocator protein. [¹¹C]PBR28 signal was quantified using standardized uptake values ratio (validated against volume of distribution ratio; n=23). Functional MRI data were collected simultaneously to the [¹¹C]PBR28 data 1) to functionally localize the primary somatosensory cortex back and leg subregions and 2) to perform functional connectivity analyses (in order to investigate possible neurophysiological correlations of the neuroinflammatory signal). PET and functional MRI measures were compared across groups, cross-correlated with one another and with the severity of “fibromyalgianess” (i.e., the degree of pain centralization, or “nociplastic pain”). Furthermore, statistical mediation models were employed to explore possible causal relationships between these three variables.

For the primary somatosensory cortex representation of back/leg, [¹¹C]PBR28 PET signal and functional connectivity to the thalamus were: 1) higher in radicular compared to axial back pain patients, 2) positively correlated with each other and 3) positively correlated with fibromyalgians scores, across groups. Finally, 4) fibromyalgians mediated the association between [¹¹C]PBR28 PET signal and primary somatosensory cortex-thalamus connectivity across groups.

Our findings support the existence of “neuroinflammatory signatures” that are accompanied by neurophysiological changes, and correlate with clinical presentation (in particular, with the degree of nociplastic pain) in chronic pain patients. These signatures may contribute to the subtyping of distinct pain syndromes and also provide information about inter-individual variability in neuro-immune brain signals, within diagnostic groups, that could eventually serve as targets for mechanism-based precision medicine approaches.

Author affiliations:

1 Department of Radiology, Athinoula A. Martinos Center for Biomedical Imaging, Massachusetts General Hospital, Harvard Medical School, Charlestown, MA, USA

2 Department of Anesthesia, Critical Care and Pain Medicine, Massachusetts General Hospital, Harvard Medical School, Boston, MA, USA

3 Medical Image Analysis and Biometry Laboratory, Universidad Rey Juan Carlos, Madrid, Spain

4 Department of Anesthesiology, Perioperative and Pain Medicine, Brigham and Women’s Hospital, Harvard Medical School, Boston, MA, USA

5 Department of Radiology, Logan University, Chesterfield, MO, USA

Correspondence to: Marco L. Loggia, PhD

Massachusetts General Hospital ,149 Thirteenth Street, Room 2301, Charlestown, MA 02129, USA

E-mail: marco.loggia@mgh.harvard.edu

Running title: Neuro-immune signatures in low back pain

Keywords: glial cells; functional connectivity; chronic pain; neuropathic; inflammation

Abbreviations: AIF = arterial input function; BMI = body mass index; CI = confidence interval; cLBP = chronic low back pain; cLBP_{AX} = axial chronic low back pain; cLBP_{RAD} = radicular chronic low back pain; CSF = cerebrospinal fluid; DV = dependent variable; DVR = ratio of distribution volume; fMRI = functional MRI; GM = grey matter; IPS = intraparietal sulcus; IV = independent variable; M = mediator; M1 = primary motor cortex; PCA = principal component analysis; PCC = posterior cingulate cortex; ROI = region of interest; S1 = primary somatosensory cortex; SSS = symptom severity score; SUV = Standardized uptake value; SUVR = Standardized uptake value ratio; TNF- α = tumor necrosis factor- α ; TSPO = 18kDa translocator protein; VPL = ventral posterior lateral nucleus; V_T = distribution volume; WM = white matter; WPI = Widespread Pain Index

Introduction

Over the past two decades, preclinical studies have implicated astrocytes and microglia in pain models, suggesting that neuro-immune responses may be key to the development and maintenance of chronic pain.¹⁻⁷ Both microglia and astrocytes are important in the defense against acute stress by restoring homeostasis,⁸⁻¹⁰ but their chronic activation poses a threat to the normal functioning of the central nervous system.^{11,12} Moreover, in animal models, glial inhibitors prevent, delay, or reverse persistent pain behaviors.¹³⁻²⁰ These observations suggest that neuro-immune activation represents a viable target in our search for novel methods of treating chronic pain.

While the role of glia in human pain remains unknown, our group, using integrated PET/MRI, has found elevated levels of 18kDa translocator protein (TSPO), a marker of glial activation, in the brain and/or spinal cord of patients with chronic low back pain (cLBP),²¹⁻²³ fibromyalgia,²⁴ migraine,²⁵ and Gulf War Illness.²⁶ Because TSPO is upregulated in activated astrocytes and microglia,²⁷⁻²⁹ this body of work suggests that neuroinflammation is likely present in human chronic pain. This thereby adds clinical evidence to the plethora of preclinical studies supporting the exploration of glial cells as possible therapeutic targets for pain.

Interestingly, different patient groups appear to present with seemingly different spatial patterns of TSPO signal elevations, i.e., distinct “neuroinflammatory signatures”. For example, we previously reported comparable TSPO signal elevations in the thalamus in two independent cohorts of cLBP patients compared to healthy controls,^{21,22} whereas in patients with fibromyalgia we observed very little thalamic involvement. Instead, fibromyalgia patients exhibited cortical TSPO signal elevation that was widespread (possibly reflecting the complex and multi-symptom nature of this disorder) and appeared to be quite similar to that observed in veterans with Gulf War Illness (paralleling the similarity in clinical presentation often observed across these two disorders).^{24,30} Along with the primary somatosensory cortex (S1), we observed elevation in TSPO signal in regions compatible with the lumbar spine cortical representation in chronic low back pain, the face area in migraine, and in a large portion of the sensorimotor strip in patients suffering from fibromyalgia, thus paralleling the body distribution of the pain (lumbar, facial and whole-body) reported in these patient groups.^{21,24,25} Collectively, these studies raise the intriguing possibility that TSPO imaging may be used to objectively characterize subtypes of patient populations based on their clinical presentation, an

important step towards the identification of disorder-specific imaging biomarkers, that could eventually serve as targets for mechanism-based precision medicine approaches.

To test the hypothesis that TSPO signal may be used to characterize subtypes of patient populations, we used PET/MRI imaging with [^{11}C]PBR28,^{31,32} a second-generation TSPO ligand,^{33,34} to investigate differences in neuroinflammatory signatures within a cohort of cLBP patients. We explored two subtypes of cLBP: patients with cLBP that radiates to the leg (radicular cLBP, cLBP_{RAD}) and patients with cLBP that does not radiate (axial cLBP, cLBP_{AX}). Typically, cLBP_{RAD} has a neuropathic component explained by damage/presumed damage to the nerve,³⁵ whereas cLBP_{AX} is usually considered non-neuropathic³⁶. Importantly, pharmacological treatments showing some efficacy in one subtype of cLBP may not work in the other,³⁶ implying different pathomechanisms in patients with different clinical presentation. However, it is currently unknown whether different cLBP subtypes demonstrate distinct neuro-immune patterns. Therefore, in the present study we explored whether cLBP_{RAD} exhibit distinct neuroinflammatory patterns compared to cLBP_{AX}. In particular, based on the abovementioned differential involvement of S1 observed in patient groups with different clinical presentations, we predicted that cLBP_{RAD} would have more pronounced neuroinflammatory signal in the S1 leg area, compared to cLBP_{AX}. To relate changes in PET signal to the cortical representations of clinically relevant body regions, we used functional MRI collected simultaneously to the PET to functionally localize the S1 back and leg subregions in these patients. Furthermore, we collected resting-state BOLD functional MRI (fMRI) data to investigate the possible functional significance of the neuroinflammatory signal. The investigation of functional connectivity in this study was motivated both by preclinical work supporting the occurrence of a bidirectional interplay between glial cells and neurons (as neuroinflammation may affect neuronal communication³⁷ and, contrariwise, neural activity may activate neuroinflammatory cells)³⁸ and by our work linking TSPO signal elevations to alterations in functional connectivity in patients with negative affect comorbid with chronic pain.³⁹

Materials and methods

Patients and Study design

Twenty-six patients with cLBP_{AX} (15 females; 43.7±16.6 years old [mean ± SD]), and 28 patients with cLBP_{RAD} (16 females; 48.3±13.2 years old) were identified from two separate

protocols. Protocol 1 (10 cLBP_{AX}: 35.1±11.5 years old; 15 cLBP_{RAD}: 47.2±12.2 years old) was a cross-sectional study while Protocol 2 (16 cLBP_{AX}: 49.1±17.3 years old; 13 cLBP_{RAD}: 49.6±14.5 years old) was a randomized, double-blind, placebo-controlled clinical trial testing the effect of a medication (ClinicalTrials.gov identifier: NCT03106740). Only baseline (i.e., pre-treatment) data from Protocol 2 were included. Data from Protocol 1 has been included in prior publications.^{21,22,39,40} However, none of these previous publications investigated differences between cLBP_{AX} and cLBP_{RAD} (i.e., the main question of the present study). Data from Protocol 2 have not previously been published.

In both protocols, patients had been diagnosed with cLBP at a minimum of six months prior to enrollment, formally confirmed and categorized into cLBP_{AX} or cLBP_{RAD} by a trained nurse practitioner (Protocol 1) or a pain physician (Protocol 2). Patients had an ongoing pain of at least 3 on a 0-10 scale, present for at least 50% of days during a typical week. Patients were excluded for history of major psychiatric illness, neurological illness, cardiovascular disease, peripheral nerve injury, routine use of benzodiazepines to avoid possible binding competition for TSPO (except clonazepam, lorazepam and alprazolam, which have a known low binding affinity for this target⁴¹⁻⁴⁵), history of substance abuse, current or past history within the last 5 years of major medical illness not affecting the CNS other than chronic pain, change in pain regimen during the enrollment period, epidural steroid injection within 3 (Protocol 1) or six weeks (Protocol 2) prior to scanning, inability to communicate in English, and contraindication for PET/MRI scanning (e.g., pacemaker, metallic implants, pregnancy). Protocol 2 had additional inclusion/exclusion criteria, requiring patients to have been on a stable pain treatment for four weeks prior to recruitment, and excluding patients receiving new interventions during enrollment period, routine use of opioids ≥ 60 mg morphine or contraindication to medication used in the clinical trial.

Both protocols were conducted at the Athinoula A. Martinos Center for Biomedical Imaging at Massachusetts General Hospital. The Institutional Review Board and the Radioactive Drug Research Committee approved these studies. All patients gave written informed consent.

Behavioral visit

All patients participated in a behavioral visit, during which a clinician completed a history and physical examination to assess eligibility and clinically characterize the patients.

During this visit, patients completed various questionnaires (see below) and venous blood or saliva was collected for genotyping of the Ala147Thr *TSPO* polymorphism, which predicts high (Ala/Ala), mixed (Ala/Thr) or low (Thr/Thr) binding affinity to the radioligand.^{46,47} Patients exhibiting the Thr/Thr genotype, i.e. , low affinity binders, were excluded from any additional study procedures, whereas those with the Ala/Ala or Ala/Thr polymorphisms could proceed to the imaging visit. Additionally, in this visit patients from protocol 2 were familiarized with the electrical stimulation (e-stim) protocol to be used during the imaging visit.

Imaging visit

For all eligible patients, brain imaging was performed with Siemens PET/MRI tomographs. Patients from Protocol 1 were imaged using a Siemens 3T Tim Trio whole-body MRI with a dedicated avalanche photodiode-based brain PET scanner (BrainPET)⁴⁸ with a spatial resolution of 2-3mm.⁴⁹ Patients from Protocol 2 were imaged using a Siemens Biograph mMR scanner, with a spatial resolution of 4-5mm.⁵⁰ The dynamic PET data were acquired in list mode and reconstructed with corrections for decay, random coincidences, detector sensitivity and scatter. Up to 15 millicuries (mCi) of [¹¹C]PBR28, produced in-house using a procedure modified from the literature⁵¹, was injected as an intravenous bolus, and dynamic PET were acquired for 90 min as described previously.^{40,52} Simultaneous with the PET, a 6-min blood oxygen level-dependent (BOLD) resting-state fMRI scan was acquired in each patient (Protocol 1: TR/TE=2s/30ms, flip angle=90°, voxel size=3.1×3.1×3mm, 37 slices; Protocol 2: TR/TE=2.3s/30ms, flip angle=90°, voxel size=3×3×3mm, 41 slices), with eyes open. Further, to localize the somatotopic representation in S1 area for the back and leg, BOLD fMRI scans concurrent with e-stim were performed in a subset of patients (n=21) from Protocol 2 (TR/TE=2.3s/30ms, flip angle=90°, voxel size=3×3×3mm, 41 slices). Detailed methods in Supplementary section.

For anatomical localization, spatial normalization, and generation of attenuation correction maps,⁵³ a multi-echo MPRAGE (T1-weighted structural MRI) volume was also acquired (TR/TE1/TE2/TE3/TE4=2530/1.64/3.5/5.36/7.22ms, flip angle=7°, voxel size=1mm isotropic).

In 23 patients (8 cLBP_{AX} and 15 cLBP_{RAD}), a radial artery catheter was inserted and blood samples were collected at 3-10s intervals for the first three minutes, followed by samples collected at 5, 10, 20, 30, 50, 70 and 90 minutes post-[¹¹C]PBR28 injection. These data were

used to perform full kinetic modeling, in order to validate the semiquantitative ratio metric used in the study (see below). Blood data were excluded from further analyses for one patient due to technical difficulties during sample collection. Detailed methods on blood metabolite analysis are included in the Supplementary section.

Behavioral measures

During either the behavioral visit (Protocol 1) or the imaging visit (Protocol 2), patients completed the PainDETECT⁵⁴ and Brief Pain Inventory⁵⁵ to assess components of pain, including intensity, interference and likelihood of a neuropathic component. A subset of patients also completed the American College of Rheumatology Fibromyalgia Survey Criteria⁵⁶⁻⁵⁸ (n=35) which is traditionally used to differentiate patients with fibromyalgia from those without (survey scores ≥ 13 and < 12 , respectively). It can also be used as a continuous measure of symptom severity, and to assess the degree of nociplastic pain (i.e. “fibromyalgianess”) in individuals who meet criteria for fibromyalgia⁵⁹ and individuals with other pain disorders who do not.^{60,61}

PET

For all patients from both protocols, PET data were corrected for radioactive decay, deadtime, variable detector sensitivity, random coincidences, photon attenuation and scatter using software provided by the manufacturer or developed in house. Attenuation correction was performed using an MR-based approach developed in house.⁵³ The PET volumes were reconstructed using a 3D ordinary Poisson ordered subset expectation maximization (OP-OSEM) algorithm provided by the manufacturer and the space-variant point spread function of the BrainPET was modeled as described in Bowen et al.⁶² To minimize the attenuation-emission mismatch, the MPRAGE volume was co-registered to the reconstructed PET volume corresponding to the 60-90-minute frame. Standardized uptake value (SUV) ratio (SUVR) images were generated from data collected over the 60-90 min post-injection [¹¹C]PBR28 PET interval, as previously described.^{40,52,63} In brief, SUV maps were computed by normalizing radioactivity by injected dose/body weight. The SUV maps were nonlinearly transformed to MNI space (MNI152), applying to these maps the transformation computed from the coregistration of MPRAGE to PET volume, and smoothed with an 8mm full width at half-maximum Gaussian kernel for consistency with prior studies,^{24,25,30,39,64} using tools from FSL (FMRIB Software Library, <http://www.fmrib.ox.ac.uk/fsl/>), AFNI (Analysis of Functional

NeuroImages, <http://afni.nimh.nih.gov/afni>), and FreeSurfer (<http://surfer.nmr.mgh.harvard.edu/>). To obtain SUVR maps, SUV maps were intensity-normalized by the mean SUV extracted from the whole-brain (i.e. an average of all brain voxels within MNI standard template), which showed no significant difference between $cLBP_{AX}$ and $cLBP_{RAD}$ ($p=0.45$), indicating that the use of this signal as a normalizing factor did not bias our analyses.

In order to further support the use of SUVR as an outcome metric in the present data, we compared the SUVR against the more quantitative distribution volume (V_T) and the ratio of distribution volume (DVR) outcome, determined using kinetic modelling, in a subset of patients ($n=23$) from whom arterial plasma data were available (Supplementary Methods; detailed methods described previously⁶⁴). A radiometabolite-corrected arterial input function (AIF) was used as the input for traditional 2-tissue-compartmental modeling⁶⁵ and V_T was computed via Logan plot analysis, from “target regions” (i.e., regions identified as statistically significant across groups in the voxelwise SUVR analyses in this study; see below) as well as the whole-brain. Then, each target region was divided by whole-brain V_T to obtain DVR. In all evaluated regions, V_T was not significantly correlated with SUVR ($r \leq 0.29$; $p > 0.05$); however, SUVR was strongly correlated with DVR in all regions ($r \geq 0.87$; $p \leq 0.0001$, Supplementary Figure. 1). These results provide further support for the use of SUVR as a viable PET metric in our study.

Functional MRI

Data from both resting-state and S1 “functional localizer” scans were pre-processed using a combination of tools from FSL, AFNI and FreeSurfer software packages. Data were corrected for slice-timing, head motion, and B0 field inhomogeneities and, for the e-stim scans, frame displacement-based motion outlier detection was applied. Data from both scans underwent brain extraction, co-registration to the MPRAGE, spatial smoothing with a 6-mm Gaussian kernel and high-pass temporal filtering (cut-off frequency = 0.008 Hz). Nonlinear transformation to MNI space was used to spatially normalize the contrast of parameter estimates and associate variance images for both resting-state and e-stim scans (see below). To reduce physiological noise in the resting-state BOLD fMRI data, MPRAGE images were segmented in probabilistic maps of gray matter (GM), white matter (WM), and cerebrospinal fluid (CSF) using SPM 12 (<http://www.fil.ion.ucl.ac.uk/spm/>). To minimize potential partial volume effects, WM and CSF masks were thresholded at 90% and eroded by one voxel. BOLD

data were masked with WM- and CSF-inclusive masks, and denoised with principal component analysis (PCA).⁶⁶

Statistical analysis

Group differences were assessed with Student's *t*-tests for continuous variables (age, clinical variables) and *chi*-square (χ^2) tests for categorical variables (sex, genotype) using Statistica (TIBCO Software Inc., v.13). Main group analyses compared all cLBP_{AX} with all cLBP_{RAD}, statistically correcting for the factor "Protocol", thus taking advantage of the larger sample size achieved when combining data. PET analyses also corrected for genotype to account for differences in binding affinity.^{46,47}

Group PET analyses were performed using two strategies. Given our specific focus on S1 (the region where we predicted group differences in [¹¹C]PBR28 signal, as mentioned above) and thalamus (the region consistently associated with [¹¹C]PBR28 signal elevation in cLBP in our previous analyses), we first performed region-of-interest (ROI) analyses using the S1 and thalamus clusters from our previous analysis²¹ as our two *a priori* ROIs. Mean [¹¹C]PBR28 signal extracted from each of these two regions was compared between cLBP_{AX} and cLBP_{RAD}, using two separate General Linear Models and an alpha level corrected for two comparisons ($0.05/2 = 0.025$). Next, a whole-brain voxelwise analysis was performed to evaluate the presence of group differences in the [¹¹C]PBR28 signal beyond the boundaries of the *a priori* ROIs, as well as to localize any effects observed in the ROI analyses with higher spatial accuracy. Voxelwise Ordinary Least Squares analysis was performed with FSL's FEAT GLM tool (www.fmrib.ox.ac.uk/fsl, version 5.0.10), a cluster-forming threshold of $Z=3.1$, and a cluster size significance threshold of $p=0.05$ to correct for multiple comparisons. To understand the potential clinical significance of S1 neuroinflammation, the S1 [¹¹C]PBR28 signal was correlated with PainDetect and Fibromyalgia Survey Scores, as these were the two behavioral measures that were significantly different across groups. For these analyses, we used Pearson's correlation coefficient, with an alpha level corrected for two comparisons ($0.05/2 = 0.025$).

To estimate brain responses to e-stim for S1 localization, general linear modeling was performed on the preprocessed fMRI data. The stimulation period, as well as anticipatory cues (See Supplementary methods), were modeled for each of the three body parts as explanatory variables in first level analyses, including 6 motion parameters (3 rotations and 3 translations)

and frames flagged as motion outliers as covariates. Resultant outputs such as parameter estimates and their variances, spatially normalized to MNI152, were then passed up to a one sample mixed effects analysis (FLAME1), to identify mean S1 back and leg activations, across the entire group of participants. To be maximally sensitive to S1 back and leg regions, which are known to be localized in the most dorsal portions of the postcentral gyrus and in the paracentral lobule,⁶⁷ these analyses were performed restricting the search area to a mask covering only the portions of the “postcentral gyrus” label from the Harvard-Oxford Cortical Atlas superior to $z = 54$ mm. In addition, using the same approach, we compared differences in S1 activations between $cLBP_{AX}$ and $cLBP_{RAD}$, in an exploratory analysis. These analyses were also performed with FSL’s FEAT GLM tool, a cluster-forming threshold of $Z=2.3$, and a cluster size significance threshold of $p=0.05$ to correct for multiple comparisons. This cluster-forming threshold was used in this analysis to measure S1 activations from the leg that were not evident at a higher threshold ($Z=3.1$). Indeed, the use of a cluster-forming threshold of $p=0.01$ (which corresponds to $Z=2.3$) with FSL FLAME1 provides an acceptable false error rate of around 5% (particularly in event related designs).⁶⁸

Because S1 demonstrated statistically significant differences in both ROI and whole-brain voxelwise analyses, and largely overlapped the somatotopic representation of S1 localized with back/leg stimuli (see Results), we performed seed-based functional connectivity analyses using the S1 cluster from the results of the voxelwise PET group analysis (see Results). Further, because our previous studies demonstrated consistent elevations in thalamic [¹¹C]PBR28 signal in $cLBP$ patients compared to controls,^{21,22} our functional connectivity analysis was restricted to a search space comprising the thalamic labels from the Harvard Oxford Subcortical Atlas (Center for Morphometric Analyses, http://www.cma.mgh.harvard.edu/fsl_atlas.html), to determine whether any thalamic regions showed stronger functional connectivity with S1 in $cLBP_{RAD}$ compared to $cLBP_{AX}$. This analysis was also performed with FSL’s FEAT GLM tool and FLAME1 (www.fmrib.ox.ac.uk/fsl, version 5.0.10), a cluster-forming threshold of $Z=3.1$, and a cluster size significance threshold of $p=0.05$ to correct for multiple comparisons. To explore its clinical significance and relationship with neuroinflammation, S1-thalamus fMRI connectivity strength (S1-thal) was correlated with the S1 [¹¹C]PBR28 PET signal, and the Fibromyalgia Survey Scores (the only behavioral measure significantly correlated with S1 [¹¹C]PBR28 PET signal; see Results). Again, for this analysis, we used a Pearson’s correlation and an alpha level corrected for two comparisons ($0.05/2 = 0.025$).

For visualization purposes, as well as for correlation analyses (see below), mean PET signal (SUVR) and mean fMRI values (contrast of parameter estimates) were extracted from the significant clusters identified in the voxelwise PET and fMRI analyses, and split in anatomically separate sub-regions using labels from the Harvard-Oxford Cortical Structural Atlas (Center for Morphometric Analyses, http://www.cma.mgh.harvard.edu/fsl_atlas.html), whenever applicable.

As both S1 [¹¹C]PBR28 signal and S1-thal connectivity correlated with each other and with Fibromyalgia Survey Scores (see Results), we performed mediation analyses in a subset of patients with available survey scores (n=35) to explore possible causal relationships between variables. We designed six mediation models using the Preacher and Hayes Indirect Mediation Analysis tool for SPSS,⁶⁹ version 24 (IBM Corp, Armonk, NY), with the following independent, mediator, and dependent variables (IV/M/DV): IV=S1 [¹¹C]PBR28 signal, M=Fibromyalgia Survey Scores, DV=S1-thal connectivity (Model 1); IV=Fibromyalgia Survey Scores, M=S1 [¹¹C]PBR28 signal, DV=S1-thal connectivity (Model 2); IV=S1-thal connectivity, M=Fibromyalgia Survey Scores, DV=S1 [¹¹C]PBR28 signal (Model 3); IV=Fibromyalgia Survey Scores, M=S1-thal connectivity, DV=S1 [¹¹C]PBR28 signal (Model 4); IV=S1-thal connectivity, M=S1 [¹¹C]PBR28 signal, DV=Fibromyalgia Survey Scores (Model 5); IV=S1 [¹¹C]PBR28 signal, M=S1-thal connectivity, DV=Fibromyalgia Survey Scores (Model 6). Unstandardized regression coefficients in this mediation Model and bootstrapped 95% confidence intervals (CIs) for total and indirect effects of the IV on the DV through M (5000 bootstrap samples) were estimated. The indirect (i.e., mediation) effect was considered statistically significant if the bias-corrected 95% CI did not include zero.

Data availability

Data will be made available upon reasonable request.

Results

Patient sample characteristics

Demographic and other key characteristics for all patients are displayed in Table 1. There was no significant difference in sex, age, *TSPO* polymorphism, injected dose, specific activity, or injected mass between the cLBP_{AX} and cLBP_{RAD} groups ($p > 0.05$). There was,

however, a significant difference in BMI across groups (cLBP_{AX}: 23.9±3.88; cLBP_{RAD}: 28.1±4.94; p= 0.001).

cLBP_{RAD} and cLBP_{AX} demonstrated similar clinical pain intensity, as measured using the Brief Pain Inventory (p=0.26). As expected by clinical subtyping, cLBP_{RAD} reported significantly higher PainDetect scores, indicative of a more likely neuropathic component, than cLBP_{AX} (p=0.004) and higher Fibromyalgia Survey Scores (p=0.02). All patients reported having perceived the electrical stimuli. Back, right leg and left leg stimuli were rated at 27.6±34.4 (mean ±SD), 30.9±29.7, and 32.4±32.5, respectively on a 0-100 pain intensity numerical rating scale. There was no significant difference in pain ratings between cLBP_{RAD} and cLBP_{AX} in any body region (p >0.05; Table 1).

PET imaging results

When evaluating ROIs from our previous [¹¹C]PBR28 PET study in cLBP patients,²¹ cLBP_{RAD} demonstrated significantly elevated [¹¹C]PBR28 PET signal compared to cLBP_{AX} in S1 (F(1,50)=5.7, p=0.04, corrected), but no significant difference was observed in the thalamus (F(1,50)=1.2, p=0.57, corrected; Figure 1). In addition, the whole-brain voxelwise group comparison revealed [¹¹C]PBR28 PET signal elevations in cLBP_{RAD} compared to cLBP_{AX} in S1 (in a cluster localized largely overlapping the one identified in our prior study, used in this study as our a-priori S1 ROI), as well as in the intraparietal sulcus (IPS), left and right WM, and the posterior cingulate cortex (PCC; Figure 2A and B). To explore the clinical significance of S1 neuroinflammation, [¹¹C]PBR28 PET signal in S1 was assessed for correlation with neuropathic and fibromyalgia symptom measures as both showed a significant difference across groups. S1 [¹¹C]PBR28 PET signal displayed a significant positive correlation with Fibromyalgia Survey Scores (r=0.43, p=0.026, corrected) but no significant correlation with PainDetect scores (r=0.25, p=0.11, corrected).

Functional MRI results

As shown in Figure 2C, e-stim of back and legs revealed the expected dorsal S1 functional activations. Notably, the portion of the postcentral gyrus commonly activated by both back and right leg demonstrated a distinct overlap with the S1 area as identified in the PET analyses, indicating that S1 neuroinflammatory signal in cLBP_{RAD} was indeed localized to the representation of back and leg. There was no significant difference in voxelwise

functional activation in $cLBP_{AX}$ compared to $cLBP_{RAD}$. Because S1 demonstrated a significantly elevated $[^{11}C]PBR28$ signal in both ROI and whole-brain voxelwise analyses, and largely overlapped the somatotopic representation of S1 localized with back/leg e-stim we focused on this region for further analyses. The S1 cluster identified in the voxelwise group differences was used as a seed to compare connectivity to the thalamus between $cLBP_{AX}$ and $cLBP_{RAD}$. $cLBP_{RAD}$ had stronger S1 connectivity to the right thalamus (in regions compatible with the ventral lateral posterior nucleus (VLp) and ventral posterior lateral nucleus (VPL) compared to $cLBP_{AX}$ (Figure 3A). Mean S1 connectivity values (Z-score) from this region is displayed in Figure 3B. No thalamic nuclei were identified with stronger S1 connectivity in $cLBP_{AX}$ than $cLBP_{RAD}$.

To test the hypothesis that higher S1 connectivity to the “neuroinflammation-prone” thalamus is accompanied by higher S1 neuroinflammatory signal, S1-thal connectivity was regressed against S1 $[^{11}C]PBR28$ PET signal. S1-thal connectivity was also regressed against the fibromyalgias scores, as this was the only behavioral measure significantly correlated with S1 $[^{11}C]PBR28$ PET signal. S1-thal connectivity displayed significant positive correlation with S1 $[^{11}C]PBR28$ PET signal ($r=0.33$, $p=0.04$, corrected) and Fibromyalgia Survey Scores ($r=0.58$, $p=0.002$, corrected; Figure 4).

Mediation between Fibromyalgia Survey Scores, PET signal, and functional connectivity

As the Fibromyalgia Survey Scores, S1 $[^{11}C]PBR28$ PET signal, and S1–thal connectivity were cross-correlated, we ran six bootstrapped mediation models to investigate whether one variable mediated the relationship between the other two. Of these six models, Model 1 (IV=S1 $[^{11}C]PBR28$ PET signal; M=Fibromyalgia Survey Scores; DV=S1-thal connectivity) reached statistical significance. This model revealed that the strength of the association between S1 $[^{11}C]PBR28$ PET signal and S1-thal connectivity (path c; $\beta \pm$ standard error: Model 1: 1.54 ± 0.74) was significantly reduced after accounting for the effects of the mediator, Fibromyalgia Survey Scores (path c'; Model 1: 0.59 ± 0.07). The bias-corrected 95% CIs for the indirect effect of S1 $[^{11}C]PBR28$ PET signal on S1-thal connectivity through Fibromyalgia Survey Scores (Model 1 (path $a \times b$; $\beta=0.95 \pm 0.37$) yielded a lower limit of 0.35 and an upper limit of 1.82. Thus, as the 95% CI range contains zero, Fibromyalgia Survey

Scores significantly mediate the association between S1 [¹¹C]PBR28 PET signal and S1-thal connectivity (Figure 6).

Discussion

Our investigations provide compelling evidence of neuroinflammatory and functional connectivity differences in subtypes of cLBP. Compared to cLBP_{AX}, cLBP_{RAD} patients showed elevated levels of TSPO, a neuroinflammatory marker, as measured with [¹¹C]PBR28 PET. TSPO signal elevations were observed in several brain structures including S1, a statistically significant region in both ROI and voxelwise analyses and overlapping functionally localized S1 representations of the back/leg. Compared to cLBP_{AX}, cLBP_{RAD} also demonstrated increased S1 functional connectivity to the thalamus, as measured with resting-state BOLD fMRI. Indeed, S1 TSPO signal and S1-thal functional connectivity were significantly correlated, an association that was statistically mediated by the levels of “fibromyalgianess”, a measure of nociplastic pain.

While this study is the first to report neuroinflammatory differences between subtypes of cLBP, our results conform to a growing body of evidence suggesting that neuroinflammation might present at least partially distinct spatial patterns of signal distribution in different pain conditions.^{21,23-25,30} For instance, in patients with widespread pain (fibromyalgia) we observed TSPO signal elevations in large portions of S1²⁴, whereas only ventral or dorsal portions of this region were involved in migraineurs²⁵ and cLBP²¹, compatible with head/face and back/leg representations respectively⁶⁷. These observations led us to hypothesize that, at least within this brain area, neuroinflammatory responses might present a somatotopic organization, paralleling the body distribution of the pain reported in each condition. In support of such hypothesis, in the present study we were able to directly show TSPO signal elevations in a portion of the postcentral gyrus overlapping with a functionally-localized representation of back and leg in cLBP_{RAD} patients (who report pain in back and leg), compared to cLBP_{AX} patients (who present pain only in the back), while thalamic signal was comparable across groups. It should be noted that when we²² recently investigated a mixed group of cLBP patients that included patients with/without leg symptoms, our results replicated the thalamic, but not cortical, TSPO signal elevations observed in our initial study (which included only patients with both back and leg symptoms)²¹. One possible reason for this discrepancy is that inflammation in regions processing only back (or, perhaps, only leg) information might be too

weak to be reliably detected, whereas inflammation in regions linked to processing of both leg and back pain may yield a stronger signal (hence the higher signal in cLBP_{RAD} compared to cLBP_{AX} in our study).

Radicular back pain is typically caused by damage to the dorsal root ganglion/roots causing inflammation and/or irritation, most commonly between L4 and S1, inducing pain that follows a dermatomal pattern to the lower extremity (i.e., thigh, calf and/or foot).³⁵ Conversely, axial pain can be caused by damage such as muscle strain, facet joints and/or disc degeneration, and the pain is mostly localized within the lower back region.³⁶ As such, cLBP_{RAD} is typically considered a chronic pain condition with a neuropathic component (a result of damage or presumed damage to the nerve), while cLBP_{AX} is more likely to be non-neuropathic in nature. Treatment for cLBP varies depending on the clinical presentation, as some pharmacological treatments may not work in all subtypes of cLBP, reflecting the mix of etiologies and symptoms that a cLBP diagnosis subsumes.³⁶ That different subtypes of cLBP have neuroinflammatory and neural signatures, as evidenced in this study, further supports that different clinical presentations may be accompanied by distinct neuro-immune mechanisms.

Our observation that S1-thal connectivity was linked to higher S1 TSPO signal is notable. The thalamus is a critical structure that transmits ascending nociceptive information to various parts of the cortex, including S1, through direct connections^{70,71} and has been found in multiple studies by our group to show consistent TSPO signal elevations in cLBP patients compared to healthy controls.^{21,22} While the mechanisms mediating the relationship between functional connectivity and inflammation remains unknown, one possibility is that elevated S1-thal connectivity in some patients (cLBP_{RAD}) may serve as a “vehicle” for neuroinflammation to spread “trans-synaptically”⁷² from the thalamic “neuroinflammatory hub” to the cortex. Indeed, microglial activation can be observed remotely from the location of the original pathological event, spreading along the affected neural pathways⁷². Notably, this trans-synaptic neuroinflammatory spread can be driven by alterations in neuronal input. For instance, in a rat model of Huntington’s Disease, neuronal hyperexcitation in the striatum of the basal ganglia (through the removal of inhibitory GABAergic input) was shown to trigger trans-synaptic microglial activation in the thalamus.⁷³ Furthermore, in rats, c-fiber stimulation in the sciatic nerve causes a connexin dephosphorylation in the spinal cord and an increase in the number of astrocyte gap junctions, a rise in astrocytic intracellular calcium concentrations within seconds, and microglial activation within minutes.^{38,74} These activated glial cells may then release excessive amounts of glutamate, causing excitotoxicity and, more pertinently,

sensitizing the neural pathways.⁷⁵ For example, capsaicin-induced sensitization of the primate spinothalamic tract was exacerbated by infusion of glutamate receptor agonists.⁷⁶ As such, continuous or aberrant excitatory input from the thalamus to S1 in cLBP_{RAD} may lead to neurogenic neuroinflammation (neuroinflammation due to aberrant neuronal activation) in S1. Interestingly, the thalamic nuclei in which we found an increased connectivity with S1 in cLBP_{RAD} compared to cLBP_{AX} largely overlaps the VPL, which transmit sensory information from the body to S1. Hence, it is possible that in some patients continuous excitatory input may be transmitted from the periphery, thereby causing neurogenic neuroinflammation.

Another means by which changes in functional connectivity may influence glial activity is through promoting stripping of dysfunctional synapses.^{77,78} Microglial cells express a variety of receptors for neurotransmitters, neuropeptides, and neuromodulators that allow these cells to respond to neuronal activity.⁷⁸ Cell culture studies have shown that stimulation of these receptors activates microglia⁷⁹ which can then remove dysfunctional synapses in the brain by engulfing presynaptic inputs.⁷⁸ For example, the complement component 1q protein, the protease enzyme, and the inflammatory cytokine tumor necrosis factor- α (TNF- α) all mediate synaptic stripping and, remarkably, are all upregulated by microglia in neuropathic pain models.⁸⁰

Conversely, the association between S1 neuroinflammation and S1-thal connectivity may reflect the effects of glial cells on neuronal communication. Preclinical models have shown that glial cells can modulate neuronal activity by expressing receptors that alter synaptic function, such as fractaline receptors (a transmembrane chemokine), which increase pro-inflammatory cytokines when activated and inhibit pro-inflammatory cytokines when attenuated.⁸¹⁻⁸³ These changes in cytokine concentration modulate presynaptic neurotransmitter release, and may contribute to changes in functional connectivity. Furthermore, in mice models of optic nerve crush, resident microglia, mediated by complement proteins (not neuronal activity), engulf synaptic material at distal targets,⁸⁴ which may modulate neuronal communication. Further, in our current mediation analysis, we found that our chosen measure of nociplastic pain, the Fibromyalgia Survey Scores, mediated the relationship between functional connectivity and [¹¹C]PBR28 PET, when functional connectivity was a dependent variable (Model 1). Therefore, our data also suggests that neuroinflammation might precede and perhaps modulate functional connectivity in this cohort, potentially as a function of the degree of nociplastic pain. Nonetheless, a broader interpretation of the mediational role of nociplastic pain warrants further investigation and validation,

particularly since the FMness data was available only in a subset of the participants evaluated in this study.

While it is possible that neurogenic inflammation is driving the difference between cLBP subtypes (mediated by the degree of nociplastic pain), other mechanisms of action must not be ignored. For example, peripheral activation of the immune response can transport cytokines such as TNF- α into the spinal cord to activate glial cells.³⁸ In the chronic constriction injury model of sciatic neuropathy, TNF- α was transported in sensory fibers from the dorsal root ganglion to the spinal cord.⁸⁵ Furthermore, lumbar spine compression in mice increased the blood-brain barrier permeability in the spinal cord and in the brain, allowing the increased entry of TNF- α and other immune cells into the brain.⁸⁶ In this study, patients with cLBP_{RAD} had a significantly higher neuropathic component than cLBP_{AX} as measured by PainDetect. This suggests peripheral nerve involvement which may drive recruitment of immune cells into the brain, thus activating the neuroinflammatory response.

Several caveats should be considered when interpreting the results of our study. For instance, the cross-sectional nature of our study makes it impossible to resolve the causality between neuroinflammation, alterations of functional connectivity and nociplastic pain. Preclinical studies, and longitudinal analyses may further enhance our understanding of the relationship between the three parameters. Moreover, our data was collected using two distinct protocols and scanners. Nonetheless, the differences between cLBP_{RAD} and cLBP_{AX} in the imaging and clinical variables observed in this analysis were still evident when protocols were split (Table 1; Supplementary Table 1). The consistency across protocols increased our confidence that the results obtained in the full datasets are not reflective of artifacts, but rather are indicative of genuine neuroimmune differences across cLBP subtypes.

It should also be noted that our results used SUVR images that only enable semiquantitative analyses as opposed to other commonly adopted alternatives (such as volume of distribution, V_T) due to the limited number of patients with arterial blood sampling. Nonetheless, we have previously utilized SUVR for quantification of [¹¹C]PBR28 PET data (using either whole-brain or localized regions) in patients with cLBP,^{21,22} fibromyalgia,³⁹ Gulf War Illness,³⁰ and other conditions. The validity of SUVR as an outcome measure for [¹¹C]PBR28 PET is supported by a growing number of studies. For instance, studies of neurodegenerative disorders have demonstrated statistically significant, reproducible and regionally-specific SUVR elevations in structures where neurodegeneration is known to occur,

such as M1 and corticospinal tracts in Amyotrophic Lateral Sclerosis^{40,63,87,88} and Primary Lateral Sclerosis⁸⁹, or the basal ganglia in Huntington's Disease,⁹⁰ or again in temporoparietal regions in Alzheimer's Disease.⁹¹ Not only are SUVR elevations colocalized with the areas known to be pathological; they can be proportional to disease severity. In Amyotrophic Lateral Sclerosis, for instance, SUVR in M1 was found to be a) positively correlated to clinical severity (upper motor neuron burden); b) positively correlated with the levels of myo-inositol (another putative marker of neuroinflammation), measured using magnetic resonance imaging; and c) negatively correlated with measures of structural integrity (cortical thickness, measured using morphometric analyses from structural MRI and fractional anisotropy, measured using diffusion tensor imaging).^{87,88,92} Collectively these data support the validity of SUVR as a measure for TSPO binding in certain populations.

In conclusion, our data support the existence of different “neuroinflammatory signatures” in patients with different clinical presentation, and that S1 neuroinflammatory signal is more pronounced in patients with higher “nociceptive” pain. Further, because S1 TSPO signal was correlated with S1-thal connectivity, our data support an association between changes in neuroinflammation and neuronal communication, possibly indicating that the observed alterations reflect neurogenic neuroinflammation. Future preclinical studies will be necessary to determine the underlying mechanisms of these relationships, and to determine whether neuroinflammation and related connectivity changes may contribute to the subtyping of distinct pain syndromes and also provide information about inter-individual variability in neuro-immune brain signals, within diagnostic groups, that could eventually serve as targets for mechanism-based precision medicine approaches.

Acknowledgements

We would like to thank Mackenzie Hymen for assistance with electrical stimulation equipment, Courtney Bergan for assistance with patient recruitment, data acquisition and logistical support, Grae Arabasz, Regan Butterfield and Shirley Hsu and the A.A. Martinos Radiochemistry team for producing and administering the radioligand.

Funding

This work was supported by 1R21NS087472-01A1 (MLL), 1R01NS095937-01A1 (MLL), 1R01NS094306-01A1 (MLL) and Department of Defense (DoD) W81XWH-14-1-0543 (MLL).

Competing interests

The authors report no competing interests.

Supplementary material

Supplementary material is available at *Brain* online.

References

1. Taylor AM, Mehrabani S, Liu S, Taylor AJ, Cahill CM. Topography of microglial activation in sensory-and affect-related brain regions in chronic pain. *Journal of neuroscience research*. 2017;95(6):1330-1335.
2. Mannelli LDC, Pacini A, Bonaccini L, Zanardelli M, Mello T, Ghelardini C. Morphologic features and glial activation in rat oxaliplatin-dependent neuropathic pain. *The Journal of Pain*. 2013;14(12):1585-1600.
3. Miyamoto K, Kume K, Ohsawa M. Role of microglia in mechanical allodynia in the anterior cingulate cortex. *Journal of Pharmacological Sciences*. 2017;134(3):158-165.
4. Tsuda M, Shigemoto-Mogami Y, Koizumi S, et al. P2X 4 receptors induced in spinal microglia gate tactile allodynia after nerve injury. *Nature*. 2003;424(6950):778-783.
5. Watkins LR, Hutchinson MR, Johnson KW. Commentary on Landry et al.: "Propentofylline, a CNS glial modulator, does not decrease pain in post-herpetic neuralgia patients: in vitro evidence for differential responses in human and rodent microglia and macrophages". *Experimental neurology*. 2012;234(2):351-353.
6. Calvo M, Bennett DL. The mechanisms of microgliosis and pain following peripheral nerve injury. *Experimental neurology*. 2012;234(2):271-282.
7. Calvo M, Dawes JM, Bennett DL. The role of the immune system in the generation of neuropathic pain. *The Lancet Neurology*. 2012;11(7):629-642.
8. Gehrmann J, Matsumoto Y, Kreutzberg GW. Microglia: intrinsic immune effector cell of the brain. *Brain research Brain research reviews*. 1995;20(3):269-287.
9. Pekny M, Wilhelmsson U, Pekna M. The dual role of astrocyte activation and reactive gliosis. *Neuroscience letters*. 2014;565:30-38.
10. Pekny M, Pekna M. Astrocyte reactivity and reactive astrogliosis: costs and benefits. *Physiological reviews*. 2014;94(4):1077-1098.
11. Hains BC, Waxman SG. Activated Microglia Contribute to the Maintenance of Chronic Pain after Spinal Cord Injury. *The Journal of Neuroscience*. 2006;26(16):4308-4317.
12. Ji R-R, Donnelly CR, Nedergaard M. Astrocytes in chronic pain and itch. *Nature Reviews Neuroscience*. 2019;20(11):667-685.
13. Ledebor A, Sloane EM, Milligan ED, et al. Minocycline attenuates mechanical allodynia and proinflammatory cytokine expression in rat models of pain facilitation. *Pain*. 2005;115(1-2):71-83.
14. Raghavendra V, Tanga F, DeLeo JA. Inhibition of microglial activation attenuates the development but not existing hypersensitivity in a rat model of neuropathy. *The Journal of pharmacology and experimental therapeutics*. 2003;306(2):624-630.
15. Li T, Chen X, Zhang C, Zhang Y, Yao W. An update on reactive astrocytes in chronic pain. *Journal of Neuroinflammation*. 2019;16(1):140.
16. Clark AK, Gentry C, Bradbury EJ, McMahon SB, Malcangio M. Role of spinal microglia in rat models of peripheral nerve injury and inflammation. *European journal of pain (London, England)*. 2007;11(2):223-230.
17. Obata H, Eisenach JC, Hussain H, Bynum T, Vincler M. Spinal glial activation contributes to postoperative mechanical hypersensitivity in the rat. *The journal of pain : official journal of the American Pain Society*. 2006;7(11):816-822.
18. LeBlanc BW, Zerah ML, Kadasi LM, Chai N, Saab CY. Minocycline injection in the ventral posterolateral thalamus reverses microglial reactivity and thermal hyperalgesia secondary to sciatic neuropathy. *Neuroscience letters*. 2011;498(2):138-142.

19. Guasti L, Richardson D, Jhaveri M, et al. Minocycline treatment inhibits microglial activation and alters spinal levels of endocannabinoids in a rat model of neuropathic pain. *Molecular pain*. 2009;5:35.
20. Padi SS, Kulkarni SK. Minocycline prevents the development of neuropathic pain, but not acute pain: possible anti-inflammatory and antioxidant mechanisms. *European journal of pharmacology*. 2008;601(1-3):79-87.
21. Loggia ML, Chonde DB, Akeju O, et al. Evidence for brain glial activation in chronic pain patients. *Brain*. 2015;138(Pt 3):604-615.
22. Torrado-Carvajal A, Toschi N, Albrecht DS, et al. Thalamic neuroinflammation as a reproducible and discriminating signature for chronic low back pain. *Pain*. 2020.
23. Albrecht DS, Ahmed SU, Kettner NW, et al. Neuroinflammation of the spinal cord and nerve roots in chronic radicular pain patients. *Pain*. 2018;159(5):968-977.
24. Albrecht DS, Forsberg A, Sandström A, et al. Brain glial activation in fibromyalgia—A multi-site positron emission tomography investigation. *Brain, behavior, and immunity*. 2019;75:72-83.
25. Albrecht DS, Mainero C, Ichijo E, et al. Imaging of neuroinflammation in migraine with aura: A [11C] PBR28 PET/MRI study. *Neurology*. 2019;92(17):e2038-e2050.
26. Alshelh Z, Albrecht DS, Bergan C, et al. In-vivo imaging of neuroinflammation in veterans with Gulf War illness. *Brain, Behavior, and Immunity*. 2020;87:498-507.
27. Chen MK, Guilarte TR. Translocator protein 18 kDa (TSPO): molecular sensor of brain injury and repair. *Pharmacology & therapeutics*. 2008;118(1):1-17.
28. Hernstadt H, Wang S, Lim G, Mao J. Spinal translocator protein (TSPO) modulates pain behavior in rats with CFA-induced monoarthritis. *Brain research*. 2009;1286:42-52.
29. Wei X-H, Wei X, Chen F-Y, et al. The upregulation of translocator protein (18 kDa) promotes recovery from neuropathic pain in rats. *J Neurosci*. 2013;33(4):1540-1551.
30. Alshelh Z, Albrecht DS, Bergan C, et al. In-vivo imaging of neuroinflammation in veterans with Gulf War illness. *Brain, Behavior, and Immunity*. 2020.
31. Brown AK, Fujita M, Fujimura Y, et al. Radiation dosimetry and biodistribution in monkey and man of 11C-PBR28: a PET radioligand to image inflammation. *Journal of nuclear medicine : official publication, Society of Nuclear Medicine*. 2007;48(12):2072-2079.
32. Briard E, Zoghbi SS, Imaizumi M, et al. Synthesis and Evaluation in Monkey of Two Sensitive 11C-Labeled Aryloxyanilide Ligands for Imaging Brain Peripheral Benzodiazepine Receptors In Vivo. *Journal of Medicinal Chemistry*. 2008;51(1):17-30.
33. Brown AK, Fujita M, Fujimura Y, et al. Radiation Dosimetry and Biodistribution in Monkey and Man of ¹¹C-PBR28: A PET Radioligand to Image Inflammation. *Journal of Nuclear Medicine*. 2007;48(12):2072-2079.
34. Briard E, Zoghbi SS, Imaizumi M, et al. Synthesis and evaluation in monkey of two sensitive 11C-labeled aryloxyanilide ligands for imaging brain peripheral benzodiazepine receptors in vivo. *J Med Chem*. 2008;51(1):17-30.
35. Patel EA, Perloff MD. Radicular Pain Syndromes: Cervical, Lumbar, and Spinal Stenosis. *Seminars in neurology*. 2018;38(6):634-639.
36. Urits I, Burshtein A, Sharma M, et al. Low Back Pain, a Comprehensive Review: Pathophysiology, Diagnosis, and Treatment. *Current Pain and Headache Reports*. 2019;23(3):23.
37. Clark AK, Gruber-Schoffnegger D, Drdla-Schutting R, Gerhold KJ, Malcangio M, Sandkühler J. Selective activation of microglia facilitates synaptic strength. *J Neurosci*. 2015;35(11):4552-4570.

38. Xanthos DN, Sandkühler J. Neurogenic neuroinflammation: inflammatory CNS reactions in response to neuronal activity. *Nature Reviews Neuroscience*. 2014;15(1):43-53.
39. Albrecht D, Kim M, Akeju O, et al. The neuroinflammatory component of negative affect in patients with chronic pain. *Molecular Psychiatry*. 2019:1-11.
40. Albrecht DS, Normandin MD, Shcherbinin S, et al. Pseudoreference Regions for Glial Imaging with (11)C-PBR28: Investigation in 2 Clinical Cohorts. *Journal of nuclear medicine : official publication, Society of Nuclear Medicine*. 2018;59(1):107-114.
41. Clow A, Glover V, Sandler M. Triazolam, an anomalous benzodiazepine receptor ligand: in vitro characterization of alprazolam and triazolam binding. *Journal of neurochemistry*. 1985;45(2):621-625.
42. Gehlert DR, Yamamura HI, Wamsley JK. Autoradiographic localization of "peripheral-type" benzodiazepine binding sites in the rat brain, heart and kidney. *Naunyn-Schmiedeberg's archives of pharmacology*. 1985;328(4):454-460.
43. Canat X, Carayon P, Bouaboula M, et al. Distribution profile and properties of peripheral-type benzodiazepine receptors on human hemopoietic cells. *Life sciences*. 1993;52(1):107-118.
44. Wamsley JK, Longlet LL, Hunt ME, Mahan DR, Alburges ME. Characterization of the Binding and Comparison of the Distribution of Benzodiazepine Receptors Labeled with [3H]Diazepam and [3H]Alprazolam. *Neuropsychopharmacology*. 1993;8(4):305-314.
45. Kalk NJ, Owen DR, Tyacke RJ, et al. Are prescribed benzodiazepines likely to affect the availability of the 18 kDa translocator protein (TSPO) in PET studies? *Synapse (New York, NY)*. 2013;67(12):909-912.
46. Owen DR, Howell OW, Tang SP, et al. Two binding sites for [3H]PBR28 in human brain: implications for TSPO PET imaging of neuroinflammation. *Journal of cerebral blood flow and metabolism : official journal of the International Society of Cerebral Blood Flow and Metabolism*. 2010;30(9):1608-1618.
47. Owen DR, Yeo AJ, Gunn RN, et al. An 18-kDa translocator protein (TSPO) polymorphism explains differences in binding affinity of the PET radioligand PBR28. *Journal of cerebral blood flow and metabolism : official journal of the International Society of Cerebral Blood Flow and Metabolism*. 2012;32(1):1-5.
48. Kolb A, Wehrl HF, Hofmann M, et al. Technical performance evaluation of a human brain PET/MRI system. *European radiology*. 2012;22(8):1776-1788.
49. Catana C, Benner T, van der Kouwe A, et al. MRI-assisted PET motion correction for neurologic studies in an integrated MR-PET scanner. *Journal of nuclear medicine : official publication, Society of Nuclear Medicine*. 2011;52(1):154-161.
50. Delso G, Fürst S, Jakoby B, et al. Performance measurements of the Siemens mMR integrated whole-body PET/MR scanner. *Journal of nuclear medicine : official publication, Society of Nuclear Medicine*. 2011;52(12):1914-1922.
51. Imaizumi M, Kim HJ, Zoghbi SS, et al. PET imaging with [11C]PBR28 can localize and quantify upregulated peripheral benzodiazepine receptors associated with cerebral ischemia in rat. *Neuroscience letters*. 2007;411(3):200-205.
52. Loggia ML, Chonde DB, Akeju O, et al. Evidence for brain glial activation in chronic pain patients. *Brain : a journal of neurology*. 2015;138(Pt 3):604-615.
53. Izquierdo-Garcia D, Hansen AE, Forster S, et al. An SPM8-based approach for attenuation correction combining segmentation and nonrigid template formation: application to simultaneous PET/MR brain imaging. *Journal of nuclear medicine : official publication, Society of Nuclear Medicine*. 2014;55(11):1825-1830.

54. Freynhagen R, Baron R, Gockel U, Tölle TR. Pain DETECT: a new screening questionnaire to identify neuropathic components in patients with back pain. *Current medical research and opinion*. 2006;22(10):1911-1920.
55. Cleeland C. Measurement of pain by subjective report. *Advances in pain research and therapy*. 1989;12:391-403.
56. Wolfe F, Clauw DJ, Fitzcharles MA, et al. Fibromyalgia criteria and severity scales for clinical and epidemiological studies: a modification of the ACR Preliminary Diagnostic Criteria for Fibromyalgia. *The Journal of rheumatology*. 2011;38(6):1113-1122.
57. Wolfe F, Clauw DJ, Fitzcharles MA, et al. The American College of Rheumatology preliminary diagnostic criteria for fibromyalgia and measurement of symptom severity. *Arthritis care & research*. 2010;62(5):600-610.
58. Wolfe F. Fibromyalgiansess. *Arthritis and rheumatism*. 2009;61(6):715-716.
59. Ellingsen DM, Beissner F, Moher Alsady T, et al. A picture is worth a 1000 words: linking fibromyalgia pain widespreadness from digital pain drawings with pain catastrophizing and brain cross-network connectivity. *Pain*. 2020;Publish Ahead of Print.
60. Brummett CM, Janda AM, Schueller CM, et al. Survey criteria for fibromyalgia independently predict increased postoperative opioid consumption after lower-extremity joint arthroplasty: a prospective, observational cohort study. *Anesthesiology*. 2013;119(6):1434-1443.
61. Harper DE, Sayre K, Schrepf A, Clauw DJ, Aronovich S. Impact of fibromyalgia phenotype in temporomandibular disorders. *Pain Medicine*. 2021.
62. Bowen SL, Byars LG, Michel CJ, Chonde DB, Catana C. Influence of the partial volume correction method on (18)F-fluorodeoxyglucose brain kinetic modelling from dynamic PET images reconstructed with resolution model based OSEM. *Physics in medicine and biology*. 2013;58(20):7081-7106.
63. Zürcher NR, Loggia ML, Lawson R, et al. Increased in vivo glial activation in patients with amyotrophic lateral sclerosis: assessed with [(11)C]-PBR28. *NeuroImage Clinical*. 2015;7:409-414.
64. Albrecht DS, Normandin MD, Shcherbinin S, et al. Pseudoreference Regions for Glial Imaging with (11)C-PBR28: Investigation in 2 Clinical Cohorts. *Journal of nuclear medicine : official publication, Society of Nuclear Medicine*. 2018;59(1):107-114.
65. Fujita M, Imaizumi M, Zoghbi SS, et al. Kinetic analysis in healthy humans of a novel positron emission tomography radioligand to image the peripheral benzodiazepine receptor, a potential biomarker for inflammation. *Neuroimage*. 2008;40(1):43-52.
66. Behzadi Y, Restom K, Liao J, Liu TT. A component based noise correction method (CompCor) for BOLD and perfusion based fMRI. *Neuroimage*. 2007;37(1):90-101.
67. PENFIELD W, BOLDREY E. SOMATIC MOTOR AND SENSORY REPRESENTATION IN THE CEREBRAL CORTEX OF MAN AS STUDIED BY ELECTRICAL STIMULATION1. *Brain*. 1937;60(4):389-443.
68. Eklund A, Nichols TE, Knutsson H. Cluster failure: Why fMRI inferences for spatial extent have inflated false-positive rates. *Proc Natl Acad Sci U S A*. 2016;113(28):7900-7905.
69. Preacher KJ, Hayes AF. Asymptotic and resampling strategies for assessing and comparing indirect effects in multiple mediator models. *Behavior research methods*. 2008;40(3):879-891.
70. Ab Aziz CB, Ahmad AH. The role of the thalamus in modulating pain. *Malays J Med Sci*. 2006;13(2):11-18.
71. Yen C-T, Lu P-L. Thalamus and pain. *Acta Anaesthesiologica Taiwanica*. 2013;51(2):73-80.

72. Banati RB, Cagnin A, Brooks DJ, et al. Long-term trans-synaptic glial responses in the human thalamus after peripheral nerve injury. *Neuroreport*. 2001;12(16):3439-3442.
73. Töpper R, Gehrmann J, Schwarz M, Block F, Noth J, Kreutzberg GW. Remote Microglial Activation in the Quinolinic Acid Model of Huntington's Disease. *Experimental neurology*. 1993;123(2):271-283.
74. Li WE, Nagy JI. Activation of fibres in rat sciatic nerve alters phosphorylation state of connexin-43 at astrocytic gap junctions in spinal cord: evidence for junction regulation by neuronal-glial interactions. *Neuroscience*. 2000;97(1):113-123.
75. Bal-Price A, Brown GC. Inflammatory Neurodegeneration Mediated by Nitric Oxide from Activated Glia-Inhibiting Neuronal Respiration, Causing Glutamate Release and Excitotoxicity. *The Journal of Neuroscience*. 2001;21(17):6480-6491.
76. Neugebauer V, Chen P-S, Willis WD. Role of Metabotropic Glutamate Receptor Subtype mGluR1 in Brief Nociception and Central Sensitization of Primate STT Cells. *Journal of Neurophysiology*. 1999;82(1):272-282.
77. Paolicelli RC, Bolasco G, Pagani F, et al. Synaptic Pruning by Microglia Is Necessary for Normal Brain Development. *Science*. 2011;333(6048):1456-1458.
78. Kettenmann H, Kirchhoff F, Verkhratsky A. Microglia: New Roles for the Synaptic Stripper. *Neuron*. 2013;77(1):10-18.
79. Kettenmann H, Hanisch U-K, Noda M, Verkhratsky A. Physiology of microglia. *Physiological reviews*. 2011;91(2):461-553.
80. Ward H, West SJ. Microglia: sculptors of neuropathic pain? *Royal Society Open Science*. 2020;7(6):200260.
81. Ren K, Dubner R. Activity-triggered tetrapartite neuron–glial interactions following peripheral injury. *Current Opinion in Pharmacology*. 2016;26:16-25.
82. Wu Y, Dissing-Olesen L, MacVicar BA, Stevens B. Microglia: Dynamic Mediators of Synapse Development and Plasticity. *Trends in Immunology*. 2015;36(10):605-613.
83. Clark AK, Gruber-Schoffnegger D, Drdla-Schutting R, Gerhold KJ, Malcangio M, Sandkühler J. Selective activation of microglia facilitates synaptic strength. *Journal of Neuroscience*. 2015;35(11):4552-4570.
84. Norris GT, Smirnov I, Filiano AJ, et al. Neuronal integrity and complement control synaptic material clearance by microglia after CNS injury. *Journal of Experimental Medicine*. 2018;215(7):1789-1801.
85. Shubayev VI, Myers RR. Axonal transport of TNF- α in painful neuropathy: distribution of ligand tracer and TNF receptors. *Journal of neuroimmunology*. 2001;114(1-2):48-56.
86. Pan W, Kastin AJ, Bell RL, Olson RD. Upregulation of Tumor Necrosis Factor α Transport across the Blood–Brain Barrier after Acute Compressive Spinal Cord Injury. *The Journal of Neuroscience*. 1999;19(9):3649-3655.
87. Alshikho MJ, Zürcher NR, Loggia ML, et al. Glial activation colocalizes with structural abnormalities in amyotrophic lateral sclerosis. *Neurology*. 2016;87(24):2554-2561.
88. Alshikho MJ, Zürcher NR, Loggia ML, et al. Integrated magnetic resonance imaging and [11C]-PBR28 positron emission tomographic imaging in amyotrophic lateral sclerosis. *Annals of neurology*. 2018;83(6):1186-1197.
89. Paganoni S, Alshikho MJ, Zürcher NR, et al. Imaging of glia activation in people with primary lateral sclerosis. *NeuroImage Clinical*. 2017;17:347-353.
90. Lois C, González I, Izquierdo-García D, et al. Neuroinflammation in Huntington's Disease: New Insights with 11C-PBR28 PET/MRI. *ACS Chemical Neuroscience*. 2018;9(11):2563-2571.
91. Lyoo CH, Ikawa M, Liow J-S, et al. Cerebellum Can Serve As a Pseudo-Reference Region in Alzheimer Disease to Detect Neuroinflammation Measured with PET

- Radioligand Binding to Translocator Protein. *Journal of Nuclear Medicine*. 2015;56(5):701-706.
92. Ratai E-M, Alshikho MJ, Zürcher NR, et al. Integrated imaging of [(11)C]-PBR28 PET, MR diffusion and magnetic resonance spectroscopy (1)H-MRS in amyotrophic lateral sclerosis. *NeuroImage Clinical*. 2018;20:357-364.

Figure legends

Figure 1 ROI analyses. Group differences in [¹¹C]PBR28 signal in a priori ROIs. A priori regions were selected as they demonstrated [¹¹C]PBR28 PET SUVR elevations in chronic low back pain patients compared to healthy controls.²¹ Average \pm standard deviation SUVR extracted showing differences between cLBP_{RAD} and cLBP_{AX} (adjusted for scanner and genotype). *significant difference between groups ($p < 0.05$). Triangle denotes data from Protocol 1, circle denotes data from Protocol 2. In this figure and subsequent figures, the range of the y-axis is set depending on the distribution of individual data points.

Figure 2 Voxel-wise group differences in [¹¹C]PBR28 signal. **A.** Maps displaying areas with significantly elevated [¹¹C]PBR28 SUVR in cLBP_{RAD} compared to cLBP_{AX} in a voxelwise analysis, adjusted for Protocol and genotype. **B.** Average \pm standard deviation SUVR extracted from several clusters identified as statistically significant in the voxelwise SUVR analysis from A (adjusted for scanner and genotype). **C.** BOLD fMRI localizing the somatotopic representation of S1 area for the Back+Leg and the overlap between Back+Leg e-stim and [¹¹C]PBR28 SUVR signal in cLBP_{RAD} > cLBP_{AX}. S1 = primary somatosensory cortex; IPS = intraparietal sulcus; WM = white matter; PCC = posterior cingulate cortex. Triangle denotes data from Protocol 1, circle denotes data from Protocol 2.

Figure 3 Thalamic voxel-wise group difference in connectivity with primary somatosensory cortex (S1). **A.** Volumetric maps displaying areas within the thalamus with significantly elevated connectivity with S1 (seed ROI displayed on top left in green) in cLBP_{RAD} compared to cLBP_{AX} in a thalamic specific voxelwise analysis. **B.** Average \pm standard deviation connectivity scores extracted from statistically significant cluster in the voxelwise connectivity analysis from A. Triangle denotes data from Protocol 1, circle denotes data from Protocol 2. Data adjusted for protocol.

Figure 4 Primary somatosensory cortex (S1) [¹¹C]PBR28 signal correlates with S1–thalamus connectivity. [¹¹C]PBR28 SUVR signal were extracted from the S1 cluster significant in the PET group comparisons (Figure 2). Connectivity scores were extracted from

the thalamic cluster significant in the S1 connectivity analyses (Figure 3). All data have been adjusted for protocol and genotype. Triangle denotes data from Protocol 1, circle denotes data from Protocol 2.

Figure 5 [¹¹C]PBR28 signal in the primary somatosensory cortex (S1) and S1-thalamus connectivity correlations with Fibromyalgia Survey Scores. *Top panel:* Average SUVR was extracted from S1 (see Figure 4 caption) and plotted against Fibromyalgia Survey Scores (data have been adjusted for scanner and genotype). *Bottom panel:* S1 – thalamus connectivity values were extracted (see Figure 4 caption) and plotted against Fibromyalgia Survey Scores (data have been adjusted for scanner). Triangle denotes data from Protocol 1, circle denotes data from Protocol 2.

Figure 6 Fibromyalgia Survey Scores mediate the relationship between S1-thalamus connectivity and S1 [¹¹C]PBR28 signal. A bootstrapped mediation analysis revealed that Fibromyalgia Survey Scores significantly mediated the relationship between S1-thalamus connectivity and S1 [¹¹C]PBR28 signal. Values within the parentheses represent bootstrap standard errors for each path. * $p < 0.05$; ** $p < 0.01$.

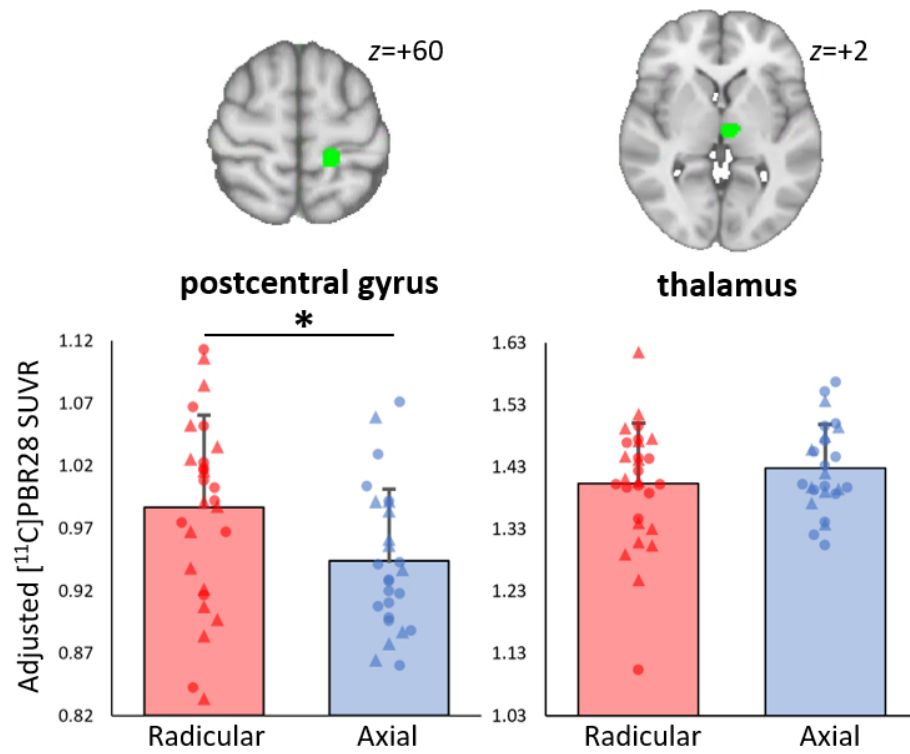


Figure 1

135x111mm (150 x 150 DPI)

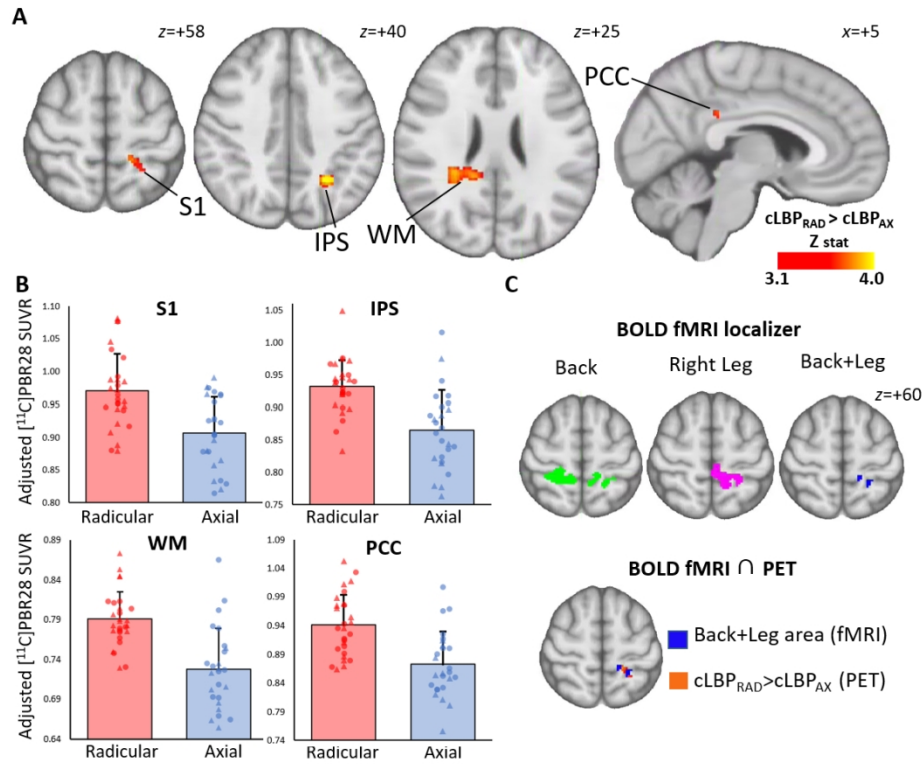


Figure 2

218x176mm (150 x 150 DPI)

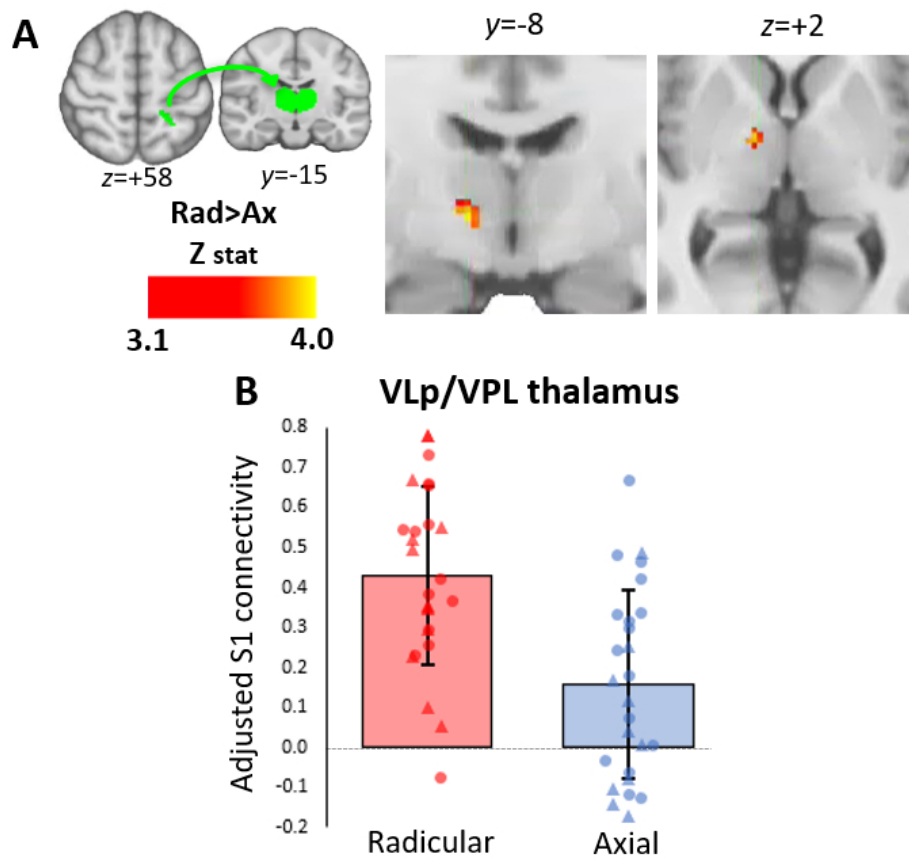


Figure 3

124x128mm (150 x 150 DPI)

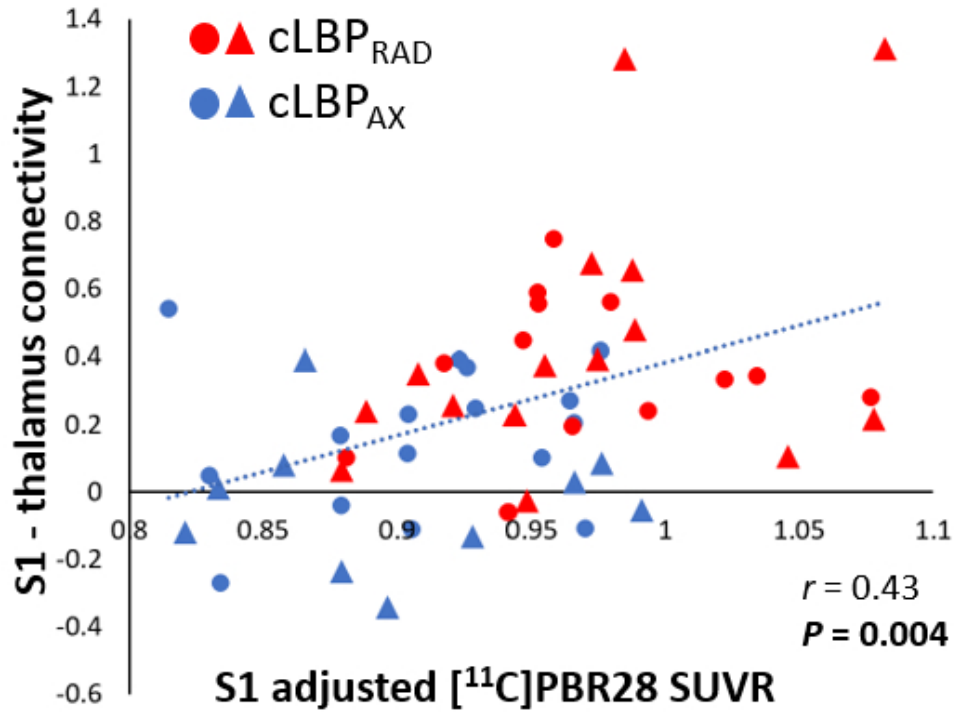


Figure 4

91x73mm (150 x 150 DPI)

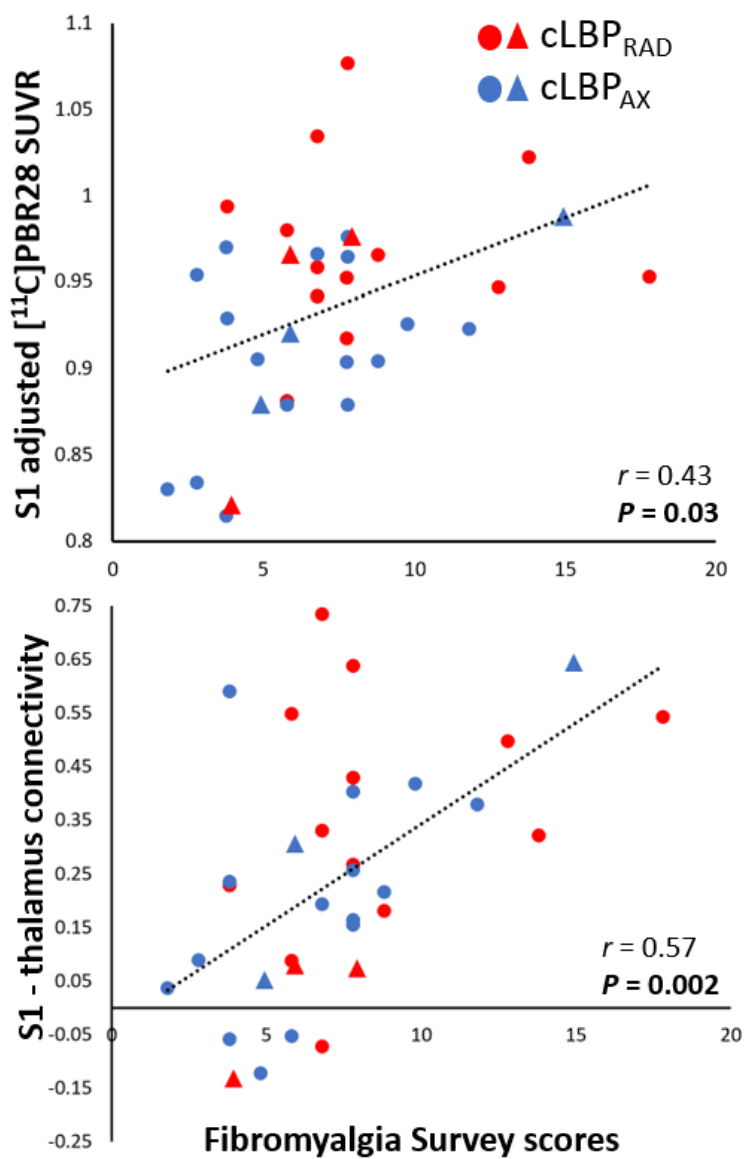


Figure 5

89x136mm (150 x 150 DPI)

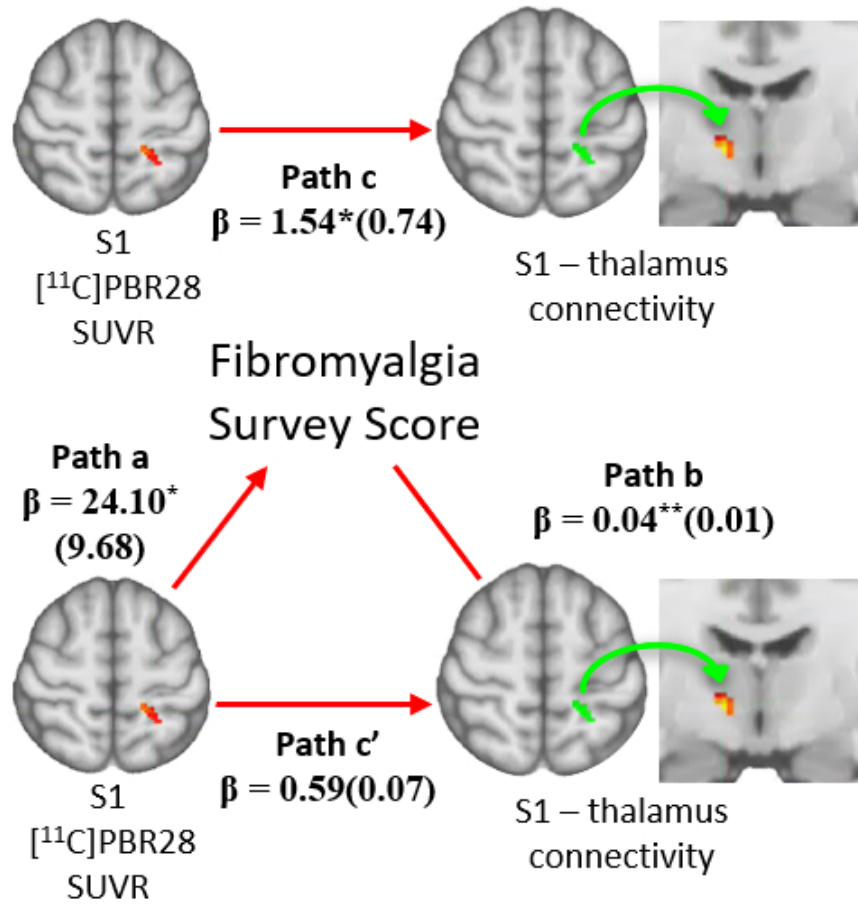


Figure 6

93x102mm (150 x 150 DPI)

Table 1 Participant characteristics

	Protocol 1		Protocol 2		Combined	
	Radicular (n=15)	Axial (n=10)	Radicular (n=13)	Axial (n=16)	Radicular (n=28)	Axial (n=26)
Age (yrs)	49.6 ± 14.5	49.1 ± 17.3	49.6 ± 14.5	49.1 ± 17.3	48.3 ± 13.2	43.7 ± 16.6
Sex	8F; 5M	10F; 6M	8F; 7M	5F; 5M	16F; 12M	15F; 11M
TSPO polymorphism	10H; 3M	12H; 4M	13H; 2M	8H; 2M	23H; 5M	20H; 6M
BMI	27.4 ± 5.6	23.6 ± 3.9	28.7 ± 4.3	24.0 ± 4.0	28.1 ± 4.9**	23.9 ± 3.9
Injected dose (MBq)	403.3 ± 45.4	432.1 ± 45.5	515.6 ± 41.1	531.0 ± 32.9	455.4 ± 71.2	492.9 ± 61.7
Specific activity (GBq/μmol)	91.7 ± 29.4	67.4 ± 23.8	43.3 ± 15.0	41.3 ± 14.9	69.2 ± 34.0	51.4 ± 22.5
Injected mass (μg)	2.4 ± 1.0	3.0 ± 2.3	5.5 ± 2.6	6.0 ± 2.7	3.8 ± 2.5	4.8 ± 2.9
PainDetect (0-38)	10.6 ± 4.5 (n=5)	9.6 ± 4.7 (n=10)	13.4 ± 4.7**	7.6 ± 4.2	12.6 ± 4.7** (n=18)	8.4 ± 4.4 (n=26)
Brief Pain Inventory (0-10)	1.1 ± 0.6 (n=12)	1.0 ± 0.3 (n=4)	3.9 ± 1.8	3.2 ± 1.8	2.6 ± 1.2 (n=25)	2.8 ± 1.9 (n=20)
Fibromyalgia Survey Scores	8.6 ± 5.5 (n=3)	5.9 ± 2.0 (n=3)	8.7 ± 3.9	6.1 ± 2.9	8.6 ± 4.0* (n=16)	6.1 ± 2.7 (n=19)
Back e-stim – Pain intensity	--	--	25.6 ± 33.9 (n=9)	29.5 ± 36.5 (n=12)	--	--
Right Leg e-stim – Pain intensity	--	--	28.1 ± 31.3 (n=9)	33.5 ± 29.6 (n=12)	--	--
Left Leg e-stim – Pain intensity	--	--	39.4 ± 27.8 (n=9)	26.0 ± 36.5 (n=12)	--	--

P* < 0.05.*P* < 0.01.

Methods

Blood metabolite analysis: For samples collected at 5, 10, 20, 30, 50, 70, and 90 minutes post- $[^{11}\text{C}]\text{PBR28}$ injection, blood was immediately separated under centrifugation (4,000 g; 4 min; 4°C) for each time point. In 18 patients, arterial blood processing was performed as previously described using a HyperSep C18 solid extraction cartridge to separation of radiometabolites.⁴⁵ In 4 patients, arterial blood was processed as follows. After centrifugation, 1 mL of plasma was added to 1 mL of acetonitrile and vortexed 3 times for 3 secs each. Protein precipitate was separated by centrifugation (4,000 g; 4 min; 4°C) then 1 mL of organic supernatant was added to 4 mL of water, vortexed, and injected (5 mL) onto High Performance Liquid Chromatography (HPLC) for separation of radiometabolites from parent radiotracer. The HPLC was configured with a column-switching valve for sample concentration (online solid phase extraction SPE; Agilent Bond Elut Online SPE, PLRP-S, 4.6 x 12.5 mm) followed by separation (Agilent Eclipse Plus C18, 4.6 x 100 mm. 3.5 μm). Configuration of the radiometabolite HPLC was modeled from previously reported methods.⁹¹ Briefly, each plasma sample was injected and trapped onto the SPE concentrator column with 1% ACN / 99% H_2O at 2mL/min for 3min. After 3 min, the sample was reverse eluted from the SPE column onto the separation column under gradient conditions (Mobile Phase A: water + 0.1% formic acid; Mobile Phase B: acetonitrile + 0.1% formic acid; separation method = 95/5 - 50/50 A/B from 3 – 8 min linear gradient; 50/50 – 5/95 A/B from 8-10 min linear gradient; 5/95 A/B from 10-11min isocratic; flow rate 2 mL/min). Radioactive analytes were monitored from 0-11 min after sample injection by dual opposing bismuth germanium oxide detectors for coincidence detection (Eckert and Ziegler). RadioHPLC chromatograms for each plasma sample analysis were decay-corrected and integrated to measure area under the curve for each radioactive metabolite compared to the parent radiotracer.

The parent fraction from each plasma sample from both analysis methods was fitted and applied to the plasma input curve resulting in a radiometabolite-corrected plasma input function. As two methods were used for blood processing in the analysis, blood was processed using both methods, and V_T was extracted from all target regions in 4 patients (1 included in this study, and 3 from different studies) to validate the use of both methods. V_T from the first blood processing method was significantly correlated against from the second blood processing method V_T ($0.995 \leq r \leq 0.999$; $p \leq 0.005$), allowing us to combine our data to increase statistical power in our study.

Electrical Stimulation: Each patient underwent two separate stimulation runs, each lasting 5 minutes 38 seconds. In each run, participants received 5 electric current stimuli, for each of the three body regions, i.e. back, right leg and left leg (pseudo-randomized order). For the back stimulation, electrodes were placed on the left and right of the fourth lumbar spine vertebra; for the right and left leg, electrodes were positioned on the lateral and medial sections of the knee. Each electrical stimulus was applied for 2 seconds at 35 Hz, at either 5mA (first run) or 12mA (second run). Stimuli were delivered using a TENS unit (Empi 300pv electrotherapy system) controlled with an in-house script using LabVIEW 16, Austin, Texas. Each stimulus was delivered 4-8s (jittered) after a visual anticipatory cue, indicating the body part about to be stimulated (indicated by the words “Back” “Right leg”, or “Left leg” projected in black onto a white background). Visual stimuli were presented using E-Prime (version 2.0). At the completion of each run, patients were asked to rate the average pain intensity (0 indicating no pain and 100 indicating worst pain tolerable) at each site. Please note that in the present study, we will only present the results of the 12mA (the strongest stimulation condition, thus more reliable to serve as a somatosensory functional localizer), whereas the 5mA run and the anticipatory cues are beyond the scope of the current investigation.